

# Modelling and simulation of relationship between internal cell temperature and apparent resistivity for lithium-ion battery

**X B Hong\*, N Z Li, W W Yin, J H Feng, G X Liu**

*College of mechanical and automotive engineering, South China University of Technology, Guangzhou, 510640 China*

*Corresponding author's e-mail: mexbhong@scut.edu.cn*

*Received 22 August 2014, www.cmnt.lv*

## Abstract

Safety problems caused by thermal runaway have been restricting the popularization and application of power lithium-ion battery (LIB). As Electrical Resistance Tomography (ERT) method can potentially detect the variations of internal cell apparent resistivity influenced by temperature, the simulation of the relationship between the internal cell temperature and apparent resistivity is presented to monitor the thermal circumstance inside LIB cell. Using the linear interpolation functions, the LIB model is built and meshed. The appropriate boundary conditions are imposed to simulate the cell virtual heating process and ERT process. During the simulations, the distributions of the apparent resistivity at different temperatures are given. It is found that the correlation of apparent resistivity and temperature is well fitted by quintic function. Meanwhile, the evaluation of quintic fit under cell discharge reveals a deviation of 6.2K between the cell core temperature and the surface temperatures. The presented method cannot only be applied in thermal balance management, life prediction and load control, but also afford a possible way for monitoring the health of separator structure of LIB.

*Keywords:* lithium-ion battery model, thermal simulation, internal cell temperature, apparent resistivity

## 1 Introduction

The lithium-ion battery (LIB) cells with the advantages of high energy density and long cycle life have been the research hotspot of the new energy automotive technology [1]. With the rapid development of new energy vehicle, an increasing number of problems on the LIB cells are frequently occurring. As a result, the related cell performance test is highly valued. As the irregular change of internal cell temperature is the roots of many security problems, such as leakage, fire, explosion, and so on, the thermal security problems of LIB cells are urgent to be resolved.

There are many researches focusing on LIB cells temperature measurements, which mainly concentrate on developing numerical models of LIB cells to estimate the core temperature. Kim et al. [2] developed a model of LIB considering the possible internal thermal reaction, which was used in the temperature field simulation of small cylindrical LIB. Then the researchers investigated mutual effect between a battery cell of thermal runaway and another normal cell [3]. It is particularly gratifying that some novel advanced techniques have been generating in recent years. Srinivasan et al. [4] (2011) proposed an Electrochemical Impedance Spectrum (EIS) method to explore the correlation between the internal cell temperature and the phase angle of electrochemical impedance at a certain frequency. The method increases the accuracy of the temperature measurement without setting up additional external sensors and wires. Subsequently, Schmidt et al. [5] (2013) investigated the sensitivity of the method on temperature and state of charge (SOC). However, these current methods can only measure or estimate the overall internal cell temperature, but cannot effectively detect the local cell temperature, which is the essence of thermal safety problems of LIB.

Electrical Resistance Tomography (ERT) method is used to assess the internal structure conditions of objects,

and has been widely applied in many fields such as concrete structure investigation, two-phase flow detection and medical inspection. For example, Paulo et al. [6] performed three dimensional detection analysis of massive concrete in different conditions using the relative excitation. Rodgers et al. [7] studied the regional network model of fluid distribution of turbulent pipeline using the adjacent excitation. Though the ERT technique has been used widely in many fields, there is little research for condition assessment of LIB cells.

The feasibility of ERT method to investigate the distribution of internal cell apparent resistivity has been validated by the authors [8]. This study aims to explore the relationship between the internal cell temperature and apparent resistivity by simulating the cell virtual heating process and ERT process. For this purpose, a steel shell LIB cell model was built and the appropriate boundary conditions were applied. Then the distribution of the cell internal temperature distribution was achieved, as well as the apparent resistivity. Finally, the correlation of the temperature and the apparent resistivity was fitted and evaluated under cell discharge in experiments.

## 2 Modelling

### 2.1 HEAT GENERATION MODEL FOR LIB CELL

Sato et al. [9] have obtained the total heat  $Q$  generated from the LIB cell and Ni-MH cell in experiments. The results show that the heat from battery mainly contains four aspects, joule heat  $Q_j$  from ohmic resistance, side reaction heat  $Q_s$  from internal waste gas, heat  $Q_p$  from electrodes polarization, and heat  $Q_r$  from chemical reaction. Generally, heat release and heat absorption occur in charge and discharge. Under a certain temperature and pressure, a constant thermodynamic relation would exist in LIB cell, and the heat energy of chemical reaction equals to the change of standard

Gibbs free energy change  $\Delta G$  of current described as follow,

$$\Delta G = \Delta H - T\Delta S, \tag{1}$$

where  $\Delta H$  and  $\Delta S$  respectively denote the enthalpy and entropy changes of chemical reaction, and  $T$  is the absolute temperature. As the processes of charge and discharge are reversible and the term  $T\Delta S$  just represents the reaction heat  $Q_r$ , which can be further expressed as,

$$Q_r = T\Delta S = T\left(-\frac{\delta\Delta G}{\delta\Delta T}\right), \tag{2}$$

where

$$\Delta G = -nFE_e, \tag{3}$$

where  $n$  denote the charge number of chemical reaction,  $F$  indicates the Faraday constant and  $E_e$  is the electromotive force of reversible cells. Furthermore,  $Q_r$  can be deduced as,

$$Q_r = nFT\left(\frac{\delta E_e}{\delta T}\right). \tag{4}$$

In normal circumstances, side reaction of waste gas would not happen, namely  $Q_s=0J$ . Therefore, the total heat  $Q$  generated from charge and discharge can be expressed as,

$$Q = Q_r + Q_j + Q_p + Q_s = nFT\left(\frac{\delta E_e}{\delta T}\right) + I^2(R_e + R_p), \tag{5}$$

where  $R_e$  and  $R_p$  are cell ohmic resistance and polarization resistance. In practical, the heat generation rate  $q$  is used for evaluating the cell thermal performance as follow,

$$q = Q / V_b, \tag{6}$$

here,  $V_b$  is the volume of battery cell. It can be seen that  $Q$  and  $q$  both correlate with reaction heat, charge and discharge current and internal resistance. In order to accurately estimate the heat generation rate and total heat produced in cell operation, these three parameters just mentioned above should be known in advance.

## 2.2 TWO DIMENSIONAL FEM MODEL OF LIB CELL

The rationale of ERT technique can be explained by electromagnetism, and a two dimensional Finite Element Method (FEM) model in electromagnetic is used to solve some engineering matters. The main concept of the FEM is based on subdividing the geometrical domain of a boundary-value problem into smaller sub-domains, called the finite elements, and expressing the governing differential equation along with the associated boundary conditions as a set of linear equations that can be solved computationally using linear algebra techniques [10]. The nodal FEM will be applied to a generic 2-dimensional (2-D) Boundary Value Problem (BVP) in electromagnetic for LIB model. Specifically, a proper application of the FEM for the solution of 2-D BVPs must involve the following major steps:

- (a) Discretization of the 2-D domain.
- (b) Derivation of the weak formulation of the governing differential equation.
- (c) Proper choice of interpolation functions.
- (d) Derivation of the element matrices and vectors.
- (e) Assembly of the global matrix system.
- (f) Imposition of boundary conditions.

(g) Solution of the global matrix system.

(h) Post-processing of the results.

Here, three of the most important steps below are considered before the modeling.

Problem definition: A BVP characterized by a generic form of a second-order partial differential equation will be considered to illustrate the major steps involved in a 2-D nodal,

$$\frac{\partial}{\partial x}\left(\alpha_x \frac{\partial u}{\partial x}\right) + \frac{\partial}{\partial y}\left(\alpha_y \frac{\partial u}{\partial y}\right) + \beta u = g, \tag{7}$$

where  $\alpha_x$ ,  $\alpha_y$ ,  $\beta$ , and  $g$  are constants to be defined by the specific application and  $u$  is the primary unknown quantity. Poisson's equation, for a linear and isotropic medium, is given by

$$\nabla(\epsilon\nabla V) = -\rho_v, \tag{8}$$

where  $\epsilon$  presents the dielectric constant,  $V$  denotes the fixed potential and  $\rho_v$  is the uniform electron volume charge density. In a 2-D space, Equation (8) is often written as

$$\frac{\partial}{\partial x}\left(\epsilon \frac{\partial V}{\partial x}\right) + \frac{\partial}{\partial y}\left(\epsilon \frac{\partial V}{\partial y}\right) = -\rho_v. \tag{9}$$

Equation (9) is a special case of the generic form given by Equation (7). Comparing these two partial differential equations would be identical if  $u=V$ ,  $\alpha_x=\alpha_y=\epsilon$ ,  $\beta=0$  and  $g=-\rho_v$ . Consequently, the 2-D Poisson's equation, which is widely used to solve electrostatic problems, is a special case of Equation (7). The set of boundary conditions could be either of Dirichlet type

$$u = u_0 \quad \text{on } \Gamma_1, \tag{10}$$

or mixed type

$$\left(\alpha_x \frac{\partial u}{\partial x} \hat{a}_x + \alpha_y \frac{\partial u}{\partial y} \hat{a}_y\right) \cdot \hat{a}_n + \gamma u = q \quad \text{on } \Gamma_2, \tag{11}$$

where  $\hat{a}_n$  is the unit vector normal to the boundary  $\Gamma_2$  and  $\gamma$ ,  $q$  are constant to be defined.

Domain discretization: The domain of a 2-D BVP usually has an irregular shape. Using the FEM, the first step is to accurately represent the physical domain of the LIB model by a set of basic shapes. In general, a triangle is used instead of a rectangle as the basic element for the meshing of the 2-D domain, the discretization error would be effectively much smaller. A linear triangular element in the  $xy$ -plane is illustrated in Fig. 1(a). The triangle consists of three vertices which correspond to the three nodes of the element.

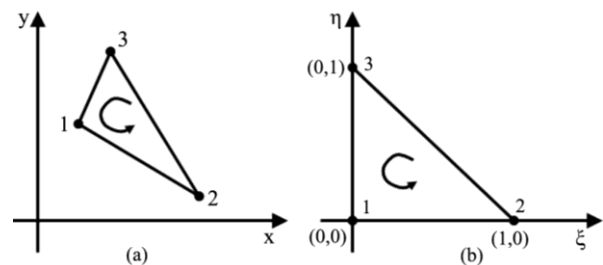


FIGURE 1 Linear triangular element respectively in the  $xy$ -plane (a) and (b) in the  $\zeta\eta$ -plane.

Interpolation functions: The nodes are locally numbered in a counter-clockwise direction to avoid having a negative area using the Jacobian definition. This element has coordinate  $(x_i^e, y_i^e)$ , which correspond to local nodes  $i = 1, 2$  and 3, respectively. A linear interpolation function spanning a triangle must be linear in two orthogonal directions. These could be the orthogonal axes defined by the natural coordinates  $\zeta$  and  $\eta$  in Fig. 1(b). For isoparametric elements, the functions used to interpolate the space coordinates  $x$  and  $y$  can be described as

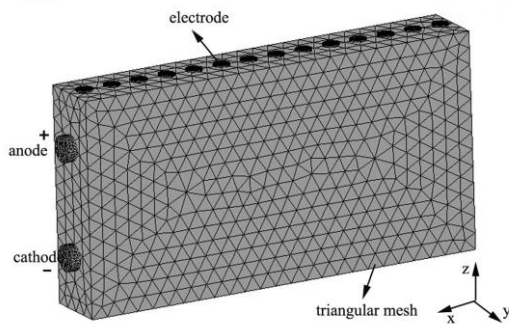
$$\begin{aligned} x &= x_1^e + \bar{x}_{21}\zeta + \bar{x}_{31}\eta \\ y &= y_1^e + \bar{y}_{21}\zeta + \bar{y}_{31}\eta \end{aligned} \tag{12}$$

where  $\bar{x}_{21} = x_2^e - x_1^e$ ,  $\bar{x}_{31} = x_3^e - x_1^e$ ,  $\bar{y}_{21} = y_2^e - y_1^e$ ,  $\bar{y}_{31} = y_3^e - y_1^e$ .

2.2 STEEL SHELL LIB MODEL



(a) Physical photo of steel shell LIB



(b) LIB model

FIGURE 2 Investigated steel shell LIB with 14 electrodes arrayed on one sides

TABLE 1 Thermal performance parameters for mainly material models

Battery component	Material	Density[kg/m <sup>3</sup> ]	Specific heat[J/kg·°C]	Heat conductivity[W/(m·°C)]	Resistivity[ohm.m]
electrolyte	PC/DEC	2335	300	$\lambda_x=1.2, \lambda_y=1.5, \lambda_z=1.0$	$10 \times 10^{-3}$
case	steel	7850	460	80	$9.78 \times 10^{-8}$
electrode	Red copper	8800	381	386.4	$1.8 \times 10^{-8}$

TABLE 2 Heat generation rates of LIB cells under different discharge rates and currents

Discharge rate [C]	Current[A]	Heat generation rate [W/m <sup>3</sup> ]
1.0	11	6335
2.0	22	19800
3.0	33	43345
4.0	44	75344
5.0	55	117725

The LIB cell with steel shell was investigated as shown in Fig. 2(a), which has a capacity of 10Ah, the maximum allowed discharge current of 40A and the internal resistance of 10mΩ. The cell size is 130\*65\*16.5mm<sup>3</sup> and the weight is 0.4Kg. Discharge cut-off voltage is 2.7V at least and the maximum charge voltage is 4.2V at most. In the right one of the Fig. 2(a), 14 electrodes have been placed on one side of the battery. The electrode is made up of red copper, which size is 10\*5\*0.2mm<sup>3</sup> and the distance between two adjacent electrodes is 9mm.

In order to synchronously produce the thermal field and the electric field, a two-dimensional hybrid model of the LIB cell is built using the ANSYS software and the mesh is divided by the linear interpolation function as discussed in Section 2. Fig.2 (b) shows the LIB cell model, which will be used in simulations below. In total, there are 14679 triangular meshes with 26132 nodes. Corresponding to Fig. 2(a), there are also 14 electrodes model placed on the cell model. The thickness of steel shell model is 0.6mm. In order to simulate the real conditions, red copper with higher conductivity than that of steel, is chosen as the cell electrode material.

3 Simulation and Analysis

3.1 THERMAL SIMULATION

The component of the LIB cell mainly consists of electrode (anode, cathode), electrolyte (mainly consists of Polycarbonate (PC) and Diethyl carbonate (DEC)), separator and cell case. Just as mentioned in Section 2, the cell internal heat mainly generates from four aspects, namely the joule heat of ohmic resistance, the side reaction of internal waste gas, the electrodes polarization and heat of chemical reaction. So the distribution of internal cell temperature can be determined by simulating with thermal specific parameters according to Table 1.

To comprehensively understand the change rule of the thermal field of the LIBs, the thermal simulation was performed to obtain the internal temperature distributions. During the process, the condition inside the LIB cell is considered as a homogeneous medium. The mass and specific heat capacity of the cell are constant and the thermal conductivity in x-y-z directions d keeps the same irrespective of the temperature and the cell capacity. The heat generation rate is consistent with a constant current in Table 2.

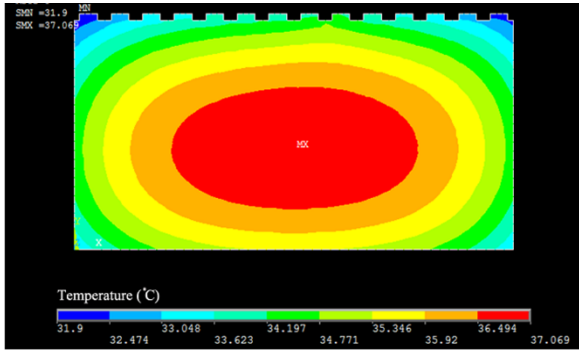


FIGURE 3 Internal cell temperature distribution in thermal simulation during discharge

In simulation, the environment temperature was set at 20°C, the battery model was discharged with the current of 1.0C discharge rate. The temperatures were recorded as the core temperature rising up 3°C. Due to the heat diffusion and convection on cell surface, the internal cell temperatures tend to be a gradient distribution. Fig.3 shows the distribution simulating at 15minutes. During the period, the internal cell temperature rises up rapidly, and the heat diffusion and convection are prominent. The internal temperatures apparently and gradiently distribute with the depth. The red area represents the highest temperature of 37°C, and the blue region represents the lowest temperature of 32°C. It is obvious that the temperatures in central place are higher than that in the verge of the cell.

3.2 ERT SIMULATION

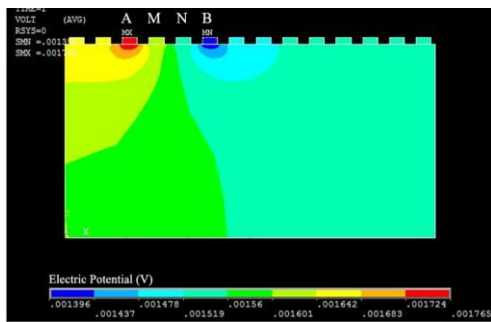


FIGURE 4 Transient of ERT simulation with four electrodes

It's important to note that the ERT simulation was performed simultaneously with the thermal simulation. The model parameters of the material resistivity were set in terms of Table 1. The boundary condition of excitation current *I* was set at 0.5mA. Before the simulations, the Wenner configuration

was chosen to excite the model. Four electrode models with a spacing of 9mm were selected to excite and measure respectively. Just as described in Fig. 4, four electrodes from the third to the sixth in the left were chosen to work, in which the bipolar pulse currents at a certain frequency were imposed on electrodes A and B. As a result, a stable electric filed is gradually produced, which is described with a variety of color ribbons in the figure. Then, the electric potential of electrodes M and N was recorded. After one set of measurements finishes, another four electrodes would be selected to repeat in the same way. The recorded electric potential difference  $\Delta U$  between the electrodes M and N can be transferred into resistivity data as

$$\rho = K \frac{\Delta U}{I}, \tag{13}$$

where *K* is the geometrical factor.

In total, four layers including twenty six data points can be obtained, which have a gradient distribution with the depth. Fig.5 shows the distribution of the apparent resistivity. It seems that the ERT method divides the internal complex structure of a battery cell into four independent levels. Each level, depending on the number of electrodes, can be further subdivided into many simple model blocks with the total number of thirty eight. The effective blocks determined by datum points would be constructed into images of apparent resistivity distribution.

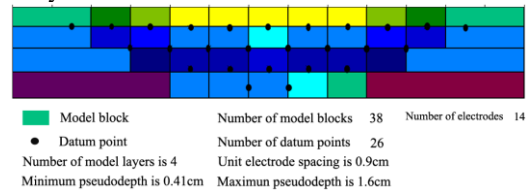


FIGURE 5 Arrangement of model blocks and datum points

Then, the distribution of the apparent resistivity at different temperatures can be achieved by the least square algorithm, which is used to reconstruct the inversion image of complex structure conditions of the objects. Fig.6 describes the apparent resistivity distribution respectively at 25°C and 30°C for LIB cell model. The two images reflect the changes of the apparent resistivity with the temperatures. It can be found that the apparent resistivity significantly distributes with the depth, more importantly, the color ribbons of same region exist obvious discrepancy with temperature. It is suggested that the relationship between the apparent resistivity and temperature can be inferred by the difference. The further analysis of fit results will be demonstrated.

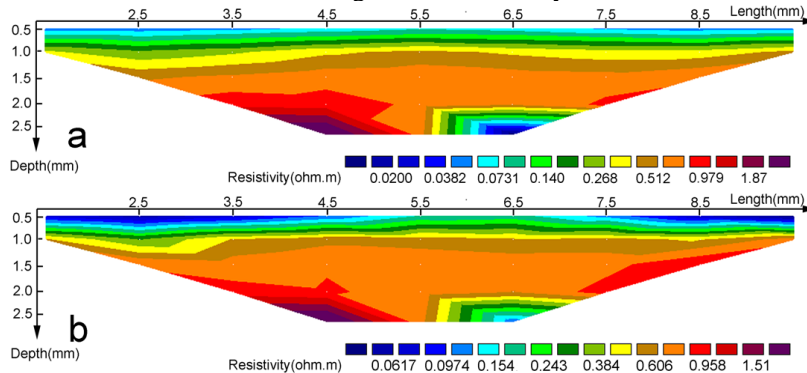


FIGURE 6 Apparent resistivity distribution of LIB cell at respectively at 25°C (a) and 30°C (b)

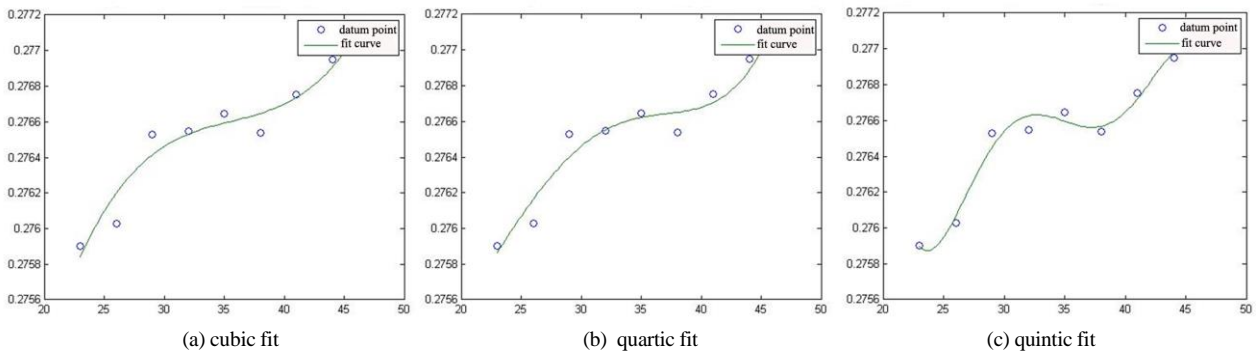


FIGURE 7 Fitted results with three different fitting methods

3.3 FITTING ANALYSIS

At the end of the simulations, the internal cell temperatures approached to 45 °C, and a set of data of the apparent resistivity and temperature has been obtained. Due to the attenuation of current density in cell deeper region, the apparent resistivity value would tend to increase up with the depth. However, the apparent resistivity value of the same depth would remain in a smaller range. Therefore, one set of the data in the first layer was chosen to analyze at first. In order to seek the relationship between the apparent resistivity and internal cell temperature, the data was fitted respectively by polynomial functions.

Here, the scatter plots of the data are presented in Fig. 7. Each data in the graphs is the average value of ten independent simulations. It can be inferred that the apparent resistivity substantially increases with the temperature rises up. This law also can be found in other data at different depth. Furthermore, it suggests that the internal cell temperature can be determined by the apparent resistivity via a certain function.

Therefore, the correlation of internal cell temperature and apparent resistivity is fitted by three different fitting functions, which are cubic fit, quartic fit and quintic fit. It can be seen that the fitting effect of the quintic fit, which has a lower mean square error of 3.06e-04, gets better than that of other two fits, 3.38e-04 for (a) cubic fit and 3.37e-04 for (b) quartic fit. As a result, this quintic function can be considered as a preliminary principle for the correlation under simulation conditions,

$$\rho = a_0T^5 + b_0T^4 + c_0T^3 + d_0T^2 + e_0T + f_0 \tag{14}$$

Herein,  $a_0$ ,  $b_0$ ,  $c_0$ ,  $d_0$ ,  $e_0$  and  $f_0$  are the fitted coefficients.

4 Evaluation under cell discharge

Usually, the core temperature would get higher than other regions in LIB cell. Evaluating the core temperature makes sense for thermal management of LIB cell. Meanwhile, in order to evaluate the quintic fit results, apparent resistivity measurements were performed under cell discharge. The experimental set-up can be seen in the Fig.8. Using the quintic function, the cell core temperature  $T_{core}$  can be determined. As there is no effective method of internal cell temperature measurements as a reference for ERT results, the calculated results will be compared with cell surface

temperatures, namely  $T_{top}$  and  $T_{bottom}$ .

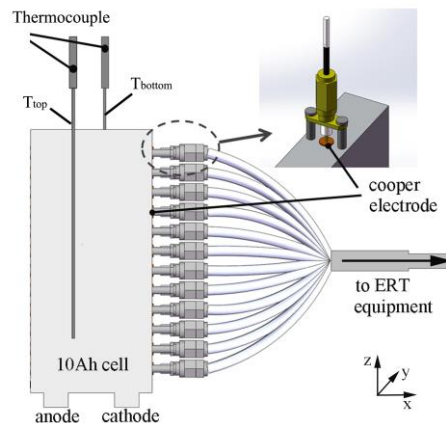


FIGURE 8 Diagram of experimental set-up

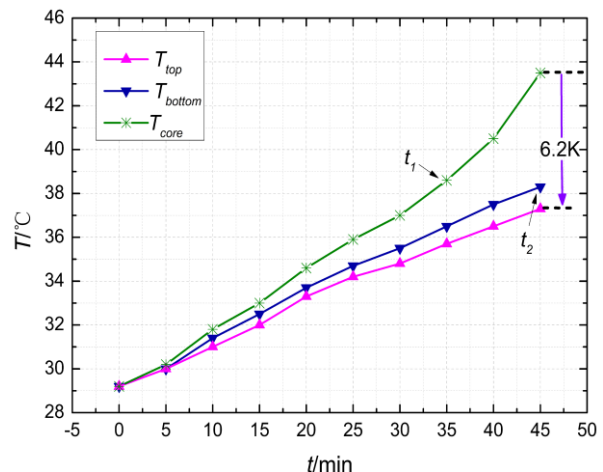


FIGURE 9 Comparison between core temperature and measured surface temperatures during LIB cells discharge (right). The initial ambient temperature was set at 30°C. Surface temperatures on top and bottom of the cell were measured with thermocouples type K

As can be observed in Fig.9, the core temperature  $T_{core}$  determined by apparent resistivity rises un normally, and do not coincide with the measured surface temperatures  $T_{top}$  and  $T_{bottom}$  especially as times goes on. After cells discharge, the core temperature reaches the highest of 43.5°C, which is 6.2K higher than  $T_{top}$ . In some degree, this is approximate to the results from a similar experiment conducted by Schmidt [5]. Meanwhile, the two surface temperatures are also not equal with each other. The temperature of top surface with 37.3°C would be almost 1k lower than that of

bottom surface. In some case, an inhomogeneous distribution of internal cell temperature is the root of the surface temperature difference. In detail, the great temperature difference could result in a great delay for heat transfer. For example, there is a delay of almost 10 minutes when  $T_{core}$  reaches to  $T_{surface}$  at  $t_1$ . This underlines the importance of local cell temperature, as already described in the Introduction.

## 5 Conclusions

This article first put forward the ERT method as a potential solution to measure the internal cell temperature for LIBs, which can be realized by the determination of the apparent resistivity on temperature. The correlation of apparent resistivity and temperature was effectively investigated by FEM simulation on steel shell LIB model.

The distribution images of the apparent resistivity indicate that the internal cell temperature significantly affects the apparent resistivity. This effect can be described by quintic fitting curve, which has been evaluated under cell

discharge. The results also reveal that the core cell temperatures significantly deviate about 6.2K from the surface temperature measured by external sensors in this experimental study. But further improvements of accuracy of this method in experimental circumstance are challenging and will have to be the subject of future works. In general, the presented method cannot only be applied in thermal balance management, life prediction and load control, but also afford a possible way for monitoring the health of separator structure of LIB cell.

## Acknowledgments

The authors thank for the support from the National Natural Science Foundation of China (NSFC) under grant No.51305141 and Guangdong-Hongkong Technology Cooperation Funding under grant No.2012A090200005 and Fundamental Research Funds Program for the Central Universities under grant No.2014ZG0016.

## References

- [1] Khare, Neeta, Rekha 2008 Modeling automotive battery diagnostics *Power Electronics Technology* **34**(3) 36-41
- [2] Kim G H, Pesaran A, Spotnitz R 2007 A three-dimensional thermal abuse model for lithium-ion cells *J. Power Sources* **170** 476-89
- [3] Kim G H, Pesaran A 2007 Analysis of heat dissipation in Li-ion cells & modules for modeling of thermal runaway *The 3rd International Symposium on Large Lithium Ion Battery Technology and Application* Long Beach, California
- [4] Srinivasan R, Carkhuff B G, Butler M H, et al. 2011 Instantaneous measurement of the internal temperature in lithium-ion rechargeable cells. *Electrochimica Acta* **56** 6198-204
- [5] Schmidt J P, Arnold S, Loges A, et al. 2013 Measurement of the internal cell temperature via impedance: Evaluation and application of a new method *J. Power Sources* **243** 110-7
- [6] Kinmoo K, Paulo J, Monteiro M 2010 Electrical Resistance Tomography imaging of concrete. *Cement and Concrete Research* **40** 137-45
- [7] Rodgers T L, Siperstein F R, Mann R, et al. 2011 Comparison of a networks-of-zones fluid mixing model for a baffled stirred vessel with three-dimensional electrical resistance tomography *Measurement Science and Technology* **22**(10) 1-12
- [8] Hong X B, Li N Z, Yin W W, et al. 2014 A novel monitoring method for internal temperature of vehicle power battery based on electrical resistance tomography *Optics and Precision Engineering* **22**(1) 193-203 (In Chinese)
- [9] Hong X B, Liu G X 2010 Double-layer compression method based on PLSR-SBR for IP mode measurement and control system. *Optics and Precision Engineering* **18**(10) 2280-87 (In Chinese)
- [10] Sato N, Yagi K 2001 Thermal Behavior Analysis of Lithium-ion Batteries for Electric and Hybrid Vehicles *J. Power Sources* **99**(1) 70-7

Authors	
	<p><b>Xiaobin Hong, born in 1979, Guangdong province, China</b></p> <p><b>Current position, grades:</b> associate professor, postgraduate tutor  <b>University studies:</b> South China University of Technology in China  <b>Scientific interest:</b> network measuring technology &amp; instruments and non-destructive detection technology  <b>Publications:</b> totally 28 publications, main publications as follow,  <b>1. 2014 <i>Optics and Precision Engineering</i> 22(1), 193-203.</b>  <b>2. 2013 <i>Smart Materials and Structure</i> 22(4),1-13</b>  <b>3. 2010 <i>Optics and Precision Engineering</i> 18(10), 2280-87.</b>  <b>Experience:</b> He received bachelor's degree at Wuhan University of technology in 2002, and doctorate at South China University of Technology in 2007, then worked in South China University of Technology. He spent one year as a visiting scholar at University of Houston in 2012.</p>
	<p><b>Nianzhi Li, born in 1989, Hubei province, China</b></p> <p><b>Current position, grades:</b> postgraduate students in second grade  <b>University studies:</b> South China University of Technology in China  <b>Scientific interest:</b> measurement techniques &amp; measuring instruments  <b>Publications:</b> one publication as follow,  <b>1.2014 <i>Optics and Precision Engineering</i> 22(1), 193-203.</b>  <b>Experience:</b> He received bachelor's degree from Wuhan University of Technology in 2012.</p>
	<p><b>Wenwei Yin, born in 1983, Guangxi province, China</b></p> <p><b>Current position, grades:</b> postgraduate students in third grade  <b>University studies:</b> South China University of Technology in China  <b>Scientific interest:</b> instrument and apparatus  <b>Publications:</b> one publication as follow,  <b>1.2014 <i>Optics and Precision Engineering</i> 22(1), 193-203.</b>  <b>Experience:</b> He received bachelor's degree from National University of Defense Technology in 2006.</p>



**Jinheng Feng, born in 1990, Guangdong province, China**

**Current position, grades:** postgraduate students in first grade

**University studies:** South China University of Technology in China

**Scientific interest:** measurement techniques & measuring instruments

**Experience:** He received bachelor's degree from Zhongkai University of Agriculture and Engineering in 2013.



**Guixiong Liu, born in 1968, Guangdong province, China**

**Current position, grades:** professor, doctoral tutor

**University studies:** South China University of Technology in China

**Scientific interest:** Intelligent sensing technology, network measuring technology, Manufacturing process quality inspection, Modeling and control.

**Publications:** 65 publications, main publications as follow,

**1. 2009 *Acta Phys. Sin.* 58(3), 2005-10.**

**2. 2008 *Acta Phys. Sin.* 57(4), 2500-04.**

**3. 2008 *Optics and Precision Engineering* 16(5), 965-971.**

**Experience:** He received bachelor's degree and doctorate at Chongqing University respectively in 1990 and 1995, now worked as a professor in South China University of Technology.